Electrical characterization of silver nanowire-graphene hybrid films from terahertz transmission and reflection measurements

Ehsan Dadrasnia, Frédéric Garet, Dongmok Lee, Jean-Louis Coutaz, Seunghyun Baik, and Horacio Lamela

Citation: Applied Physics Letters **105**, 011101 (2014); doi: 10.1063/1.4889091
View online: http://dx.doi.org/10.1063/1.4889091
View Table of Contents: http://scitation.aip.org/content/aip/journal/apl/105/1?ver=pdfcov
Published by the AIP Publishing

Electrical characterization of silver nanowire-graphene hybrid films from terahertz transmission and reflection measurements

Ehsan Dadrasnia,[1] Frédéric Garet,[2] Dongmok Lee,[3] Jean-Louis Coutaz,[2] Seunghyun Baik,[3] and Horacio Lamela[1,a)]
[1]*Optoelectronics and Laser Technology Group (GOTL), Carlos III de Madrid University, 28911 Leganes, Madrid, Spain*
[2]*IMEP-LAHC, UMR CNRS 5130, University of Savoie, 73376 Le Bourget du Lac Cedex, France*
[3]*Center for Integrated Nanostructure Physics, Institute for Basic Science (IBS), Department of Energy Science, School of Mechanical Engineering, Sungkyunkwan University, Suwon 440-746, South Korea*

(Received 11 April 2014; accepted 26 June 2014; published online 7 July 2014)

We determined the electrical sheet conductivity of silver nanowire-graphene hybrid films from transmission and reflection terahertz time-domain spectroscopy measurements. The sheet resistance extracted from noncontact terahertz measurement is in good agreement with one measured with a classical 4-point-probe technique. The conductivity is well described by a Drude-Smith model and is calculated to peak around 10 THz. © *2014 AIP Publishing LLC*.
[http://dx.doi.org/10.1063/1.4889091]

Because of their unique electrical, optical, and mechanical properties,[1,2] carbon nanotubes and graphene (GRP) have been introduced in numerous electronic devices, such as field-effect transistors,[3] super-capacitors[4] or as conductive flexible adhesives.[5] Silver nanowires (AgNWs) are flexible materials with excellent electrical conductivity.[6–8] Recently, new AgNW-GRP transparent conducting hybrid films have been intensively investigated in view of the developing of DNA sensor,[9] biological,[10] and optoelectronic devices.[11]

A comprehensive knowledge of the electrical conduction in GRP and AgNW-GRP hybrid films, as well as a precise measurement of their optical and electrical parameters, is compulsory for designing optimized electronic components. Commonly, contact devices are employed to characterize the electrical response of such films.[12–14] However, the contacting issue may damage the fragile thin films and thus may prevent a multiple measurement procedure and/or a subsequent use of the tested devices. Therefore, a non-contact and non-destructive technique are needed in practice.[15] Among modern techniques, terahertz time-domain spectroscopy (THz-TDS) is known for years to be a precise tool for non-contact characterization of samples like semiconductor wafers,[16] paint films,[17] art and historical pieces,[18] biological tissues,[19] etc.

We have recently characterized the electrical conductivity of GRP using THz-TDS transmission technique.[20] In the present paper, we use this broadband technique to determine the complex conductivity of AgNW-GRP films deposited over a quartz substrate without damaging the samples. This conductivity is extracted from transmission and reflection THz-TDS data, which allows us to minimize possible errors due to a variation of the substrate thickness between different samples. The experimental conductivity needs to be described by the Drude model as modified by Smith (DS model). This means that free charges in the AgNW-GRP films encounter a pronounced scattering against the film defects.

GRP was grown on a raw copper foil (Nilaco, 99.96%, and 100–μm thick) using chemical vapor deposition (CVD) with CH_4 and H_2 flow at 1000 °C. A typical GRP synthesis procedure using CVD is provided elsewhere.[21] The synthesized GRP films were then transferred onto fused quartz substrates (20×20 mm^2, thickness 0.54 mm) following the wet transfer method published previously.[21–23] First, polymethyl methacrylate (PMMA, from Sigma-Aldrich (46 mg/ml)) dissolved in chlorobenzene was spin-coated on the GRP/Cu substrate followed by drying at room temperature. The GRP grown on the back side of the Cu substrate was removed by oxygen plasma. The Cu substrate was then etched by using Cu etchant (Transgene, CE-100) for 1 h. The PMMA/GRP was washed by using deionized (DI) water for 1 h followed by 0.5 M hydrogen chloride treatment to remove iron nanoparticle residues. The PMMA/GRP film was rinsed with DI water for 2 h. Finally, the PMMA/GRP was transferred onto the fused quartz substrate, and PMMA was removed using acetone for 5 min. For AgNW-GRP hybrid films, AgNWs dispersed in ethanol (Nanopyxis, 1.23 mg/ml) were spin-coated onto the fused quartz substrate at 1000 rpm for 60 s followed by a 6-h drying at room temperature. The average length and diameter of AgNWs were 25 μm and 35 nm, respectively. Finally, the CVD-synthesized GRP was transferred on top of spin-coated AgNWs using the same wet transfer method. The dc electrical resistance was measured by a classical 4-point-probe technique.[24] The measurement was carried out 1500 times, and the average value was used for analysis. The thickness d of the AgNW-GRP hybrid films was measured by atomic force microscopy (AFM), and the average value was used to calculate the conductivity [Fig. 1(a)]. Two samples were characterized during this work AgNW-GRP (I) ($d = 59$ nm) and AgNW-GRP (II) ($d = 38$ nm). Fig. 1(b) shows the scanning electron microscope (SEM) image and energy dispersive X-ray (EDX) analysis of AgNW-GRP (I). The strong silicon and oxygen peaks came from the quartz substrate. Both carbon and silver peaks could be observed where AgNWs were on GRP (Spectrum 2) whereas only a carbon peak was present on the GRP surface without AgNW (Spectrum 1).

a)horacio@ing.uc3m.es

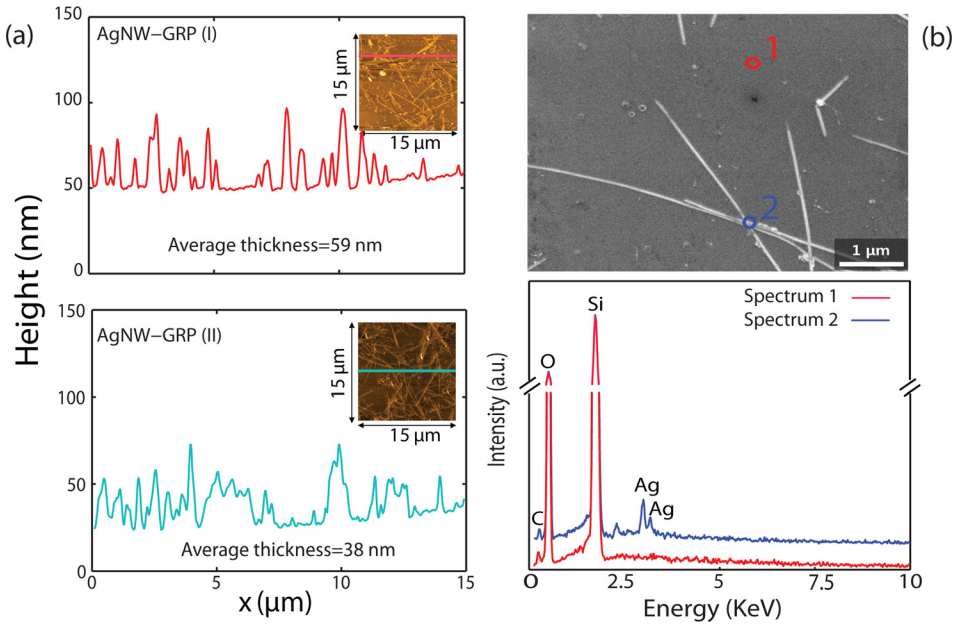

FIG. 1. (a) The surface profiles of two AgNW-GRP hybrid films. AFM images are provided as inset. (b) The SEM image and EDX analysis of AgNW-GRP (I) (d = 59 nm).

We have previously described [20,25] our classical home-made non-contact transmission and reflection THz-TDS setup. The samples are located at the waist of the THz beam. At any frequency of the available THz signal, the Rayleigh length of the beam is much larger than the bare or covered substrate. Therefore, the sample can be considered as illuminated at normal incidence by a plane wave. To execute a transmission THz differential analysis, three measurements have been performed for each film: one without the sample E_{Air}, one with a bare substrate $E_{S,T}$, and finally one $E_{F,T}$ with the substrate covered with GRP or AgNW-GRP hybrid film [Fig. 2(c)]. Each measurement was repeated several times, in order to check the reproducibility of the measurement and to reduce the experimental noise in the temporal time-domain signal [Fig. 2(a)]. The THz spectrum of the waveform measured is obtained through a numerical Fast Fourier transform. To simplify the extraction of the composite parameters, an appropriate time-windowing of the substrate and sample waveforms have been done, which rejects the echoes resulting from rebounds in the substrate.[26] The complex transmission of sample (film/substrate), whose amplitude and phase are, respectively, ρ_T and φ_T, writes

$$\tilde{T} = \rho_T\, e^{-j\varphi_T} = \frac{E_{F,T}}{E_{S,T}} \approx \left(1 + Z_0 \frac{\tilde{\sigma}_f}{1+n_s}\right)^{-1}, \qquad (1)$$

where the subscripts S and F designate the signals measured, respectively, for reference substrate and substrate covered by

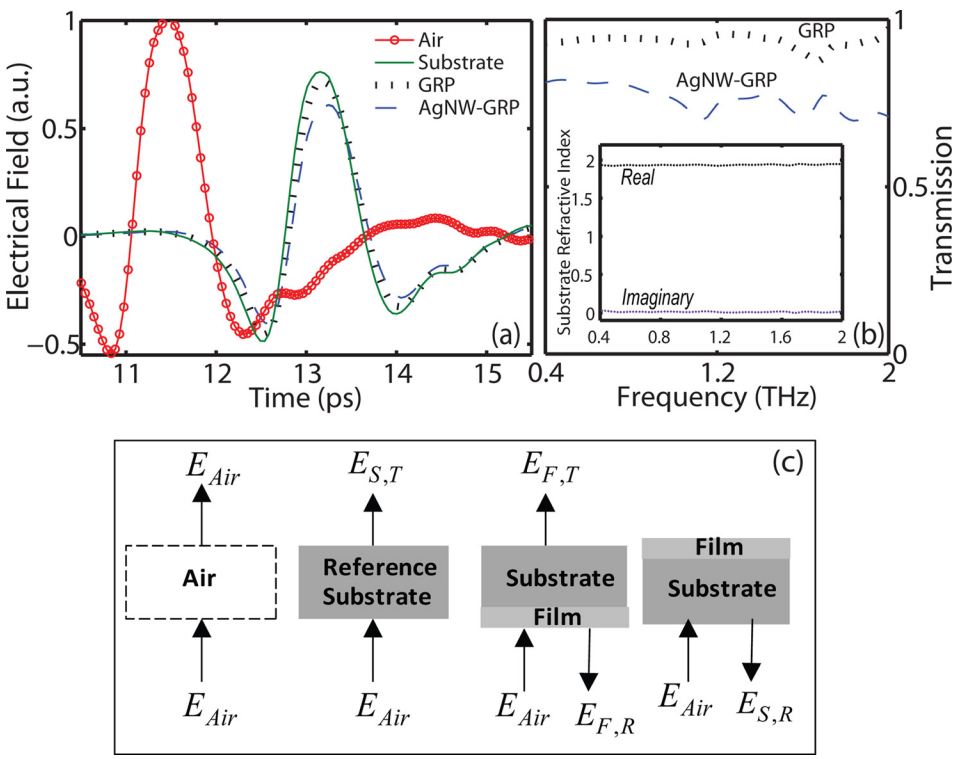

FIG. 2. (a) Measured THz temporal signals. (b) Transmission spectra of GRP and AgNW-GRP hybrid films. Inset shows the extracted imaginary and real parts of the complex refractive index of the fused quartz substrate. (c) The schematic of THz transmission and reflection measurements performed for reference, bare substrate, and substrate covered with GRP or AgNW-GRP hybrid films.

hybrid film. Z_0 is the vacuum (surrounding medium) impedance, $\tilde{\sigma}_f = \sigma_r + j\sigma_i$ is the complex sheet conductivity of the film. n_s is the refractive index of the substrate and is equal to 1.94 over the whole THz range of interest, as determined from E_{Air} and $E_{S,T}$. The power absorption of the substrate increases continuously with frequency to reach 8 cm^{-1} at 2 THz,[27] therefore the corresponding extinction, i.e., the imaginary part of the refractive index, remains very small (0.01 at 2 THz) [inset of Fig. 2(b)]. The real and imaginary parts of sheet conductivity can be easily obtained from (1)

$$\sigma_r = \frac{1+n_s}{Z_0}\left(\frac{\cos\varphi_T}{\rho_T} - 1\right), \tag{2}$$

$$\sigma_i = \frac{1+n_s}{Z_0}\frac{\sin\varphi_T}{\rho_T}. \tag{3}$$

Nevertheless, there might be a large uncertainty in this determination of $\tilde{\sigma}_f$ because the substrates of the reference sample and the film-covered sample are different, and even if they are close, their thicknesses could show a difference much bigger than the nanometric film thickness.[28] To overcome this issue, we have also measured the phase φ_R and amplitude ρ_R of the THz beam reflected by the samples using the THz-TDS setup in a reflection scheme at a normal incidence. We first measured the signal reflected $E_{F,R}$ by the covered side of the sample and then, we put the sample upside-down, and we recorded the signal reflected $E_{S,R}$ by the bare side of the sample. In both cases, only the first reflected pulse by the film is saved. The ratio of the spectra of both signals is

$$\tilde{R} = \rho_R e^{-j\varphi_R} = \frac{E_{F,R}}{E_{S,R}} \approx \frac{1 - Z_0\dfrac{\tilde{\sigma}_f}{1+n_s}}{1 - Z_0\dfrac{\tilde{\sigma}_f}{1+n_s}}. \tag{4}$$

As in the transmission case, the film conductivity is deduced from the measured coefficient (4)

$$\sigma_r = \frac{1}{Z_0}\frac{1+n_s-2n_s\rho_R\cos\varphi_R-(1-n_s){\rho_R}^2}{\dfrac{1+n_s}{1-n_s}+2\rho_R\cos\varphi_R+\dfrac{1-n_s}{1+n_s}{\rho_R}^2}, \tag{5}$$

$$\sigma_i = \frac{2}{Z_0}\frac{\rho_R\sin\varphi_R}{\dfrac{1+n_s}{1-n_s}+2\rho_R\cos\varphi_R+\dfrac{1-n_s}{1+n_s}{\rho_R}^2}. \tag{6}$$

The main issue of reflection THz-TDS is associated with the error caused by an even weak misalignment of sample, i.e., position shift as compared to the reference mirror and/or angle of incidence not exactly equal to 0°. These uncertainties will affect the achieved optical properties of the films (refractive index and absorption) and consequently their electrical conductivity. To minimize these misalignment errors, the measurement was repeated several times and both mirror and samples were removed and replaced in the setup prior to each measurement. Then, we used in the calculation the average amplitude and phase of all these recorded THz waveforms.

Fig. 2(b) shows the transmission of the samples. Both GRP (~ 90%) and AgNW-GRP hybrid (~76%) films show an almost constant transmission value up to 1.5 THz. For higher frequencies, there are some fluctuations due to the insufficient THz power. From these data, the conductivity of the films is determined using relation (2). It is important to note that, in the THz range, absorption through intraband transitions dominates the one related to interband transitions,[29] and thus intraband absorption influences mainly the THz conductivity. From now on, in this study, we consider only the contribution of intraband transitions to the conductivity of GRP. For such a free carrier population, the Drude model is typically employed for fitting the THz conductivity. However, here the Drude model modified by Smith,[20,30] which permits a better fit of the experimental THz conductivity of both GRP and AgNW-GRP hybrid films. In the DS model, the non-random scattering of the free carriers is taken into account and the expression of the complex surface conductivity $\tilde{\sigma}$ writes

$$\tilde{\sigma} = \frac{\tilde{\sigma}_f}{d} = \frac{\sigma_{dc}}{1-i\omega\tau}\left(1 + \sum_{m=1}^{\infty}\frac{c_m}{(1-i\omega\tau)^m}\right), \tag{7}$$

where d is the thickness of the film. The coefficient c_m is the fraction of the electron original velocity that is retained after the m^{th} collision. If $c_m = 0$, the carrier momentum is totally randomized (classical model by Drude). If $c_m = -1$, the free carrier is completely backscattered.[31] Fig. 3 presents the experimental surface conductivity $\tilde{\sigma}$ of GRP monolayer deposited on a quartz substrate determined from transmission THz-TDS. The conductivity obtained from reflection measurements is also plotted on Fig. 3. Even if noisier as expected because of the weaker sensitivity of extraction from reflection THz-TDS data, the surface conductivities obtained from both transmission and reflection records are in good agreement, validating the values we obtained in transmission and thus the right substrate thickness value we input in the calculation. The experimental data are well fitted with the DS model, in which $c_m = 0$, i.e., the conductivity behaves as a Drude-like one. As the corresponding plasma frequency ($f_p = 583$ THz) lies in the visible range, both real and imaginary parts of the THz sheet conductivity of GPR are almost constant (Fig. 3).

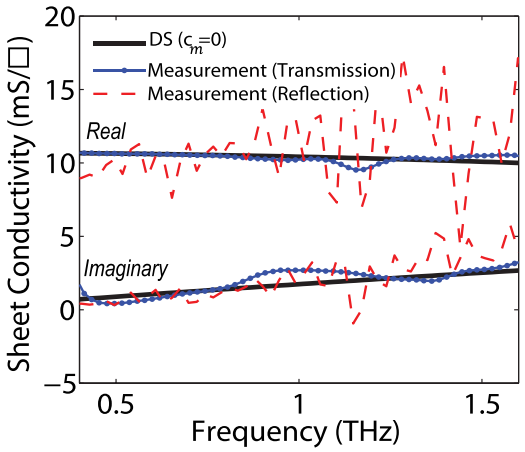

FIG. 3. Real and imaginary parts of the sheet conductivity of GRP films versus frequency as determined from THz-TDS measurement (dotted and dashed lines) and fitting curves (continuous lines).

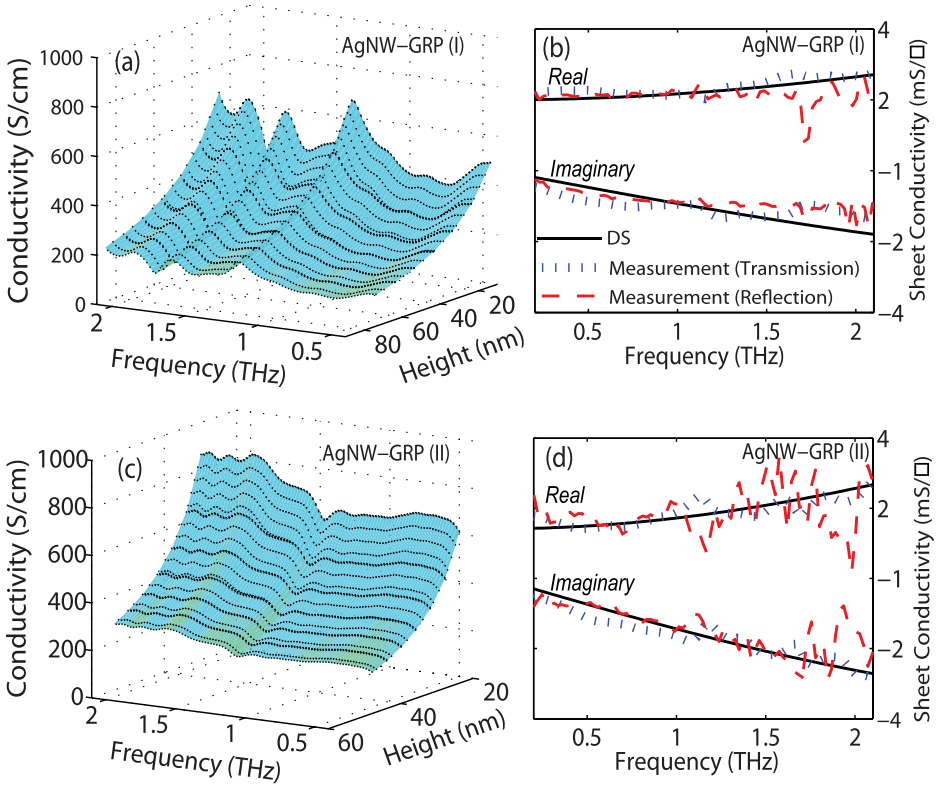

FIG. 4. (a) and (c) Real conductivity of AgNW-GRP hybrid films as function of frequency and thickness determined from transmission THz-TDS. (b) and (d) Real and imaginary parts of the sheet conductivity of AgNW-GRP hybrid films versus frequency. Dotted lines: transmission data; dashed lines: reflection data (marker lines); continuous lines: fitted curves calculated with the average film thickness shown in Fig. 1(a).

Conductivity in the AgNW-GRP is more complex than in GRP. It is strongly dependent on polarization and on the different orientations of the nanowires inside the films.[32] The THz conductivity is dominated by the contribution of the micro-structured nanowires oriented along the THz electrical field. Indeed, the lengths of the wires are comparable to the THz wavelength and thus the wires can be resonantly excited by the incoming THz field. On the other hand, due to their nanometer-scale diameter, the wires are insensitive to a THz E-field perpendicular to them. Figs. 4(a) and 4(c) depict the real part of conductivity as functions of frequency and thickness of thin films. Let us notice that the thickness of the film is not constant and exhibits peaks at given locations, due to the nanowires. Thus, Figs. 4(a) and 4(c) are plotted versus the average value of the film thickness. These experimental plots show a capacitive behavior due to electron scattering effects in the junctions of AgNW networks. The complex sheet conductivity of the films, deduced from Figs. 4(a) and 4(c), is given in Figs. 4(b) and 4(d). As the imaginary part of THz sheet conductivity decreases while increasing frequency, the conductivity model cannot be explained by a simple Drude response, but it is well fitted by the DS model (relation 7). Table I gives the parameters of the fits (plasma frequency f_p, scattering time τ and c_m coefficient) for GRP and two AgNW-GRP hybrid films. The scattering time τ is comparable to the one of noble metals and the plasma frequency is much higher than the exciting THz frequency. In the thinner film (AgNW-GRP (I), the scattering time is slightly shorter than in the thicker AgNW-GRP (II), resulting in a larger sheet resistance: this could be due to a difference of filling fractions of AgNWs or/and to the contribution of scattering at the film surfaces. c_1 is close to -1 in AgNW-GRP, which means that most of the electrons are backscattered during a collision. These collisions certainly occur at the surface of the nanowires as the carrier mean-free path is of the order of the nanowires diameter.[8] The quite small sheet conductivity in these films, as compared to GRP, is due to a smaller charge carrier density in AgNW-GRP.

To validate our results, the sheet resistance ρ $(=1/d\sigma_{dc})$ of the hybrid films was measured with a classical 4-point-probe technique, using a Keithley 6221 current source and a Keithley 2182 A nanovoltmeter. Even though the 4-point probe technique is always difficult to implement when dealing with thin films (the probes may mechanically damage the film at the contact location), the measured ρ (column 5 of Table I) is very close to the average values deduced from THz-TDS conductivity models (column 6 of Table I).

The small differences in the values of ρ given in Table I may originate in not-optimized contacts during the 4-probe measurements, but also from uncertainties in the THz-TDS study, mostly due to a bad knowledge of the thickness of the different layers. As our conductivity DS model is validated by comparison with experimental data in the THz range, we have computed the optical sheet conductivity of the AgNW-GRP hybrid films up to the UV domain, i.e., from 0.1 to 10^3 THz. A clear maximum of conductivity appears in between 9 and 11 THz (Fig. 5). It originates in the resonant behavior of the

TABLE I. THz fitting parameters used in the DS model (f_p: plasma frequency, τ: scattering time, ρ: sheet resistance). The sheet resistance measured using 4-point probe contact method is also provided for comparison.

Sample	f_p (THz)	τ (fs)	c_1	4-probe ρ (Ω/□)	DS Model ρ (Ω/□)
GRP	583	26	0 (Drude)	1055	944
AgNW-GRP (I)	232	16	−0.92	56	56
AgNW -GRP (II)	294	14	−0.87	75	65

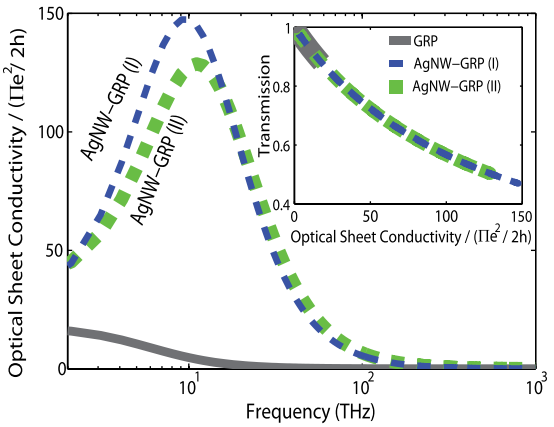

FIG. 5. Sheet conductivity of GRP and AgNW-GRP hybrid films versus frequency calculated using the Drude and Drude Smith models. The sheet conductivity is normalized by the fine-structure constant ($\pi e^2/2h$). Inset shows the calculated THz transmission of the samples as a function of the normalized sheet conductivity.

Drude and DS models, through the term $(1 - i\omega\tau)$. The peak conductivity is about 20 times larger than for GRP at 10 THz. Even around 1 THz, i.e., in the non-resonant regime, the sheet conductivity of the AgNW-GRP films (60–70 $\Omega/\square$) is comparable with the one of indium tin oxide (ITO, $\sim$80 $\Omega/\square$), making these films a good flexible conductive material for replacing indium tin oxide in many electronic applications.

In conclusion, the electrical properties of the GRP and AgNW-GRP hybrid films were characterized from non-contact transmission and reflection THz-TDS data. The measured electrical conductivity is well described by the DS model, in which a large fraction of free electrons encounter backward scattering during collisions. The hybrid structure including GRP and AgNW layers reduces the overall sheet resistance as compared to single pristine GRP films.

This work was supported by the European Community in MITEPHO (MIcrowave and TErahertz PHOtonics) project (238393 ITN-FP7). We also acknowledge the Human Resources Development program (No. 20124010203270) of the KETEP grant funded by the Korean government Ministry of Knowledge Economy.

[1]S. Bae, H. Kim, Y. Lee, X. Xu, J.-S. Park, Y. Zheng, J. Balakrishnan, T. Lei, H. Ri Kim, Y. I. Song, Y.-J. Kim, K. S. Kim, B. Ozyilmaz, J.-H. Ahn, B. H. Hong, and S. Iijima, Nat. Nanotechnol. **5**(8), 574–578 (2010).
[2]E. Dadrasnia, S. Puthukodan, and H. Lamela, J. Nanophotonics **8**(1), 083099 (2014).
[3]H. R. Byon and H. C. Choi, J. Am. Chem. Soc. **128**(7), 2188–2189 (2006).
[4]D. Yu and L. Dai, J. Phys. Chem. Lett. **1**(2), 467–470 (2010).
[5]R. Ma, S. Kwon, Q. Zheng, H. Y. Kwon, J. I. Kim, H. R. Choi, and S. Baik, Adv. Mater. **24**(25), 3344–3349 (2012).
[6]Z. Yu, Q. Zhang, L. Li, Q. Chen, X. Niu, J. Liu, and Q. Pei, Adv. Mater. **23**(5), 664–668 (2011).
[7]L. Cai-Hong and Y. Xun, Nanoscale Res. Lett. **6**(1), 75 (2011).
[8]J. Kim, I. Maeng, J. Jung, H. Song, J.-H. Son, K. Kim, J. Lee, C.-H. Kim, G. Chae, M. Jun, Y. Hwang, S. Jeong Lee, J.-M. Myoung, and H. Choi, Appl. Phys. Lett. **102**(1), 011109 (2013).
[9]X. Liu, F. Wang, R. Aizen, O. Yehezkeli, and I. Willner, J. Am. Chem. Soc. **135**(32), 11832–11839 (2013).
[10]I. Ocsoy, M. L. Paret, M. A. Ocsoy, S. Kunwar, T. Chen, M. You, and W. Tan, ACS Nano **7**(10), 8972–8980 (2013).
[11]D. Lee, H. Lee, Y. Ahn, Y. Jeong, D.-Y. Lee, and Y. Lee, Nanoscale **5**(17), 7750–7755 (2013).
[12]M.-S. Lee, K. Lee, S.-Y. Kim, H. Lee, J. Park, K.-H. Choi, H.-K. Kim, D.-G. Kim, D.-Y. Lee, S. Nam, and J.-U. Park, Nano Lett. **13**(6), 2814–2821 (2013).
[13]K. C. Fong, E. E. Wollman, H. Ravi, W. Chen, A. A. Clerk, M. D. Shaw, H. G. Leduc, and K. C. Schwab, Phys. Rev. X **3**(4), 041008 (2013).
[14]A. Anish Madhavan, S. Kalluri, D. K. Chacko, T. A. Arun, S. Nagarajan, K. R. V. Subramanian, A. Sreekumaran Nair, S. V. Nair, and A. Balakrishnan, RSC Adv. **2**(33), 13032–13037 (2012).
[15]S. Puthukodan, E. Dadrasnia, V. K. T. Vinod, H. K. Nguendon, H. Lamela, G. Ducournau, J.-F. Lampin, F. Garet, J.-L. Coutaz, D. M. Lee, and S. Baik, Electron. Lett. **50**(4), 297 (2014).
[16]D. M. Mittleman, J. Cunningham, M. C. Nuss, and M. Geva, Appl. Phys. Lett. **71**(1), 16–18 (1997).
[17]T. Yasui, T. Yasuda, K. Sawanaka, and T. Araki, Appl. Opt. **44**(32), 6849–6856 (2005).
[18]J. Labaune, J. B. Jackson, S. Pages-Camagna, I. N. Duling, M. Menu, and G. A. Mourou, Appl. Phys. A: Mater. Sci. Process. **100**(3), 607–612 (2010).
[19]E. Castro-Camus, M. Palomar, and A. A. Covarrubias, Sci. Rep. **3**, 2910 (2013).
[20]E. Dadrasnia, H. Lamela, M. B. Kuppam, F. Garet, and J.-L. Coutaz, Adv. Condens. Matter Phys. **2014**, 370619.
[21]X. Li, W. Cai, J. An, S. Kim, J. Nah, D. Yang, R. Piner, A. Velamakanni, I. Jung, E. Tutuc, S. K. Banerjee, L. Colombo, and R. S. Ruoff, Science **324**(5932), 1312–1314 (2009).
[22]G. H. Han, F. Güneş, J. J. Bae, E. S. Kim, S. J. Chae, H.-J. Shin, J.-Y. Choi, D. Pribat, and Y. H. Lee, Nano Lett. **11**(10), 4144–4148 (2011).
[23]S. Bhaviripudi, X. Jia, M. S. Dresselhaus, and J. Kong, Nano Lett. **10**(10), 4128–4133 (2010).
[24]K.-Y. Chun, Y. Oh, J. Rho, J.-H. Ahn, Y.-J. Kim, H. R. Choi, and S. Baik, Nat. Nanotechnol. **5**(12), 853–857 (2010).
[25]M. Bernier, F. Garet, and J. Coutaz, IEEE Trans. Terahertz Sci. Technol. **3**(3), 295–301 (2013).
[26]L. Duvillaret, F. Garet, and J. L. Coutaz, IEEE J. Sel. Top. Quantum Electron. **2**(3), 739–746 (1996).
[27]H. Lamela, E. Dadrasnia, D.-M. Lee, S. Baik, M. B. Kuppam, F. Garet, and J.-L. Coutaz, Proc. SPIE **8462**, 84620C (2012).
[28]L. Duvillaret, F. Garet, and J.-L. Coutaz, Appl. Opt. **38**(2), 409–415 (1999).
[29]B. Sensale-Rodriguez, Y. Rusen, L. Lei, D. Jena, and H. G. Xing, Proc. IEEE **101**(7), 1705–1716 (2013).
[30]N. V. Smith, Phys. Rev. B **64**(15), 155106 (2001).
[31]J. Lloyd-Hughes and T. I. Jeon, J. Infrared, Millimeter, Terahertz Waves **33**(9), 871–925 (2012).
[32]J. H. Strait, P. A. George, M. Levendorf, M. Blood-Forsythe, F. Rana, and J. Park, Nano Lett. **9**(8), 2967–2972 (2009).